

# A 3D Acid Transport Model For Acid Fracturing Treatments With Viscous Fingering

Rencheng Dong and Mary F. Wheeler, The University of Texas at Austin; Kang Ma, CNOOC Research Institute Co., Ltd.; Hang Su, China University of Petroleum (Beijing)

Copyright 2020, Society of Petroleum Engineers

This paper was prepared for presentation at the SPE Annual Technical Conference and Exhibition originally scheduled to be held in Houston, Texas, USA, 27-29 October 2020. Due to COVID-19 the physical event was changed to a virtual event. The official proceedings were published online on 27 October 2020.

This paper was selected for presentation by an SPE program committee following review of information contained in an abstract submitted by the author(s). Contents of the paper have not been reviewed by the Society of Petroleum Engineers and are subject to correction by the author(s). The material does not necessarily reflect any position of the Society of Petroleum Engineers, its officers, or members. Electronic reproduction, distribution, or storage of any part of this paper without the written consent of the Society of Petroleum Engineers is prohibited. Permission to reproduce in print is restricted to an abstract of not more than 300 words; illustrations may not be copied. The abstract must contain conspicuous acknowledgment of SPE copyright.

#### **Abstract**

In acid fracturing treatments, the goal is to create enough fracture roughness through differential acid etching on fracture walls such that the acid fracture can keep open and sustain a high enough acid fracture conductivity under the closure stress. The viscous fingering phenomenon has been utilized in acid fracturing treatments to enhance the differential acid etching. For relatively homogeneous carbonate reservoirs, by injecting a low-viscosity acid into a high-viscosity pad fluid during acid fracturing, the acid tends to form viscous fingers and etch fracture surfaces non-uniformly. In order to accurately predict the acid-fracture conductivity, a detailed description of the rough acid-fracture surfaces is required. In this paper, we developed a 3D acid transport model to compute the geometry of acid fracture for acid fracturing treatments with viscous fingering. The developed model couples the acid fluid flow, reactive transport and rock dissolution in the fracture. Our simulation results reproduced the acid viscous fingering phenomenon observed from experiments in the literature. During the process of acid viscous fingering, high-conductivity channels developed in the fingering regions. We performed parametric studies to investigate the effects of pad fluid viscosities and acid injection rates on acid fracture conductivity. We found that a higher viscosity pad fluid and a higher acid injection rate help acid to penetrate deeper in the fracture and result in a longer etched channel.

#### Introduction

More than 60% of the world's oil reserves and 40% of the world's gas reserves are located in carbonate reservoirs[1]. Acid stimulation is used extensively to enhance the production of oil and gas in carbonate reservoirs. There are two categories of carbonate acid stimulation: matrix acidizing and acid fracturing[2]. Since carbonate is very reactive, acid stimulation has proven to be cost effective in the field.

Matrix acidizing is mainly used to bypass damage zones and connect the reservoir and wellbores. After drilling and completion operations, some solids and fluids may invade the formation, causing formation damage like that shown in **Fig. 1a**. In matrix acidizing, strong acids such as hydrochloric acid (HCl) are injected under formation fracture pressure to dissolve the calcite mineral and create long, highly conductive channels known as wormholes, illustrated in **Fig. 1b**. Wormhole growth usually occurs within several meters around the wellbore. In the lab experiment, wormholes can be created by injecting acid into the rock

block. Wormholes can be characterized by CT scanning large blocks from acidizing lab experiments[3]. The radial wormhole from acidizing experiments is shown in **Fig. 2a**. Wormhole growth has also been modeled by solving the coupled flow and reactive transport equations in the porous medium[4, 5, 6]. The wormhole from numerical simulations is shown in **Fig. 2b**.



Figure 1: Illustration of matrix acidizing

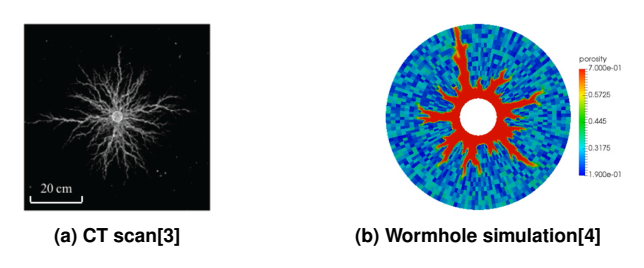


Figure 2: Wormhole characterization from experiments and simulations

Acid fracturing is another important technique to stimulate production in carbonate reservoirs. In acid fracturing operations, acid is injected at a higher pressure than formation fracture pressure. Here, a pad fluid such as a gel is first injected to break down the formation and create a desired fracture geometry. The acid is then injected after the pad stage to etch the fracture surface. Another comparable fracturing technique is hydraulic or proppant fracturing[2, 7]. The main difference between acid and proppant fracturing is how the fracture conductivity is created. In hydraulic fracturing, the proppant is injected with a fracturing fluid such as a gel to keep the induced fracture open. An illustration of the propped fracture is shown in **Fig. 3a**. The acid fracture conductivity is created by rough fracture surfaces resulting from non-uniform acid etching illustrated in **Fig. 3b**. Non-uniform acid etching on fracture surfaces can be induced by reservoir heterogeneity[8] and acid viscous fingering[9]. At the end of acid fracturing operations, the acid fracture is expected to be partially open with the support of asperities on fracture surfaces under closure stress of the formation. The residual fracture width gives rise to acid fracture conductivity, demonstrated in **Fig. 3c**.

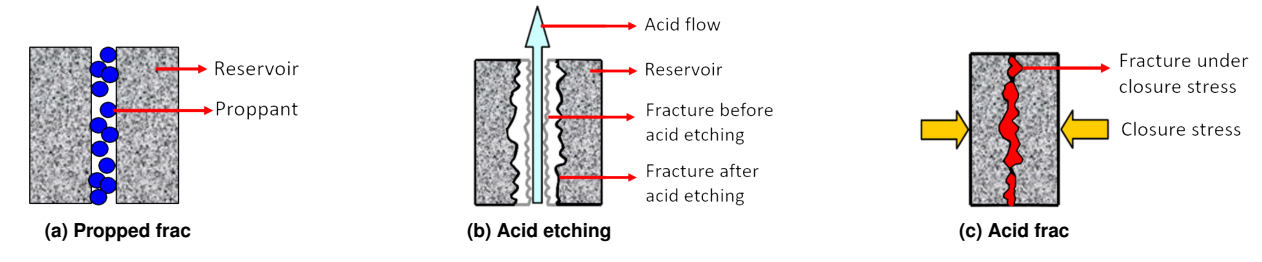


Figure 3: Illustrations of propped frac and acid frac

Non-uniform or differential acid etching is the key to creating acid fracture conductivity. For heterogeneous reservoirs, different mineralogy and permeability result in different reaction rates and non-uniform acid etching along the fracture surface. For some relatively homogeneous reservoirs, the viscous fingering technique is commonly adopted to enhance non-uniform acid etching. A typical pumping schedule

is demonstrated in **Fig. 4a** [10]. A viscous pad fluid such as gel is injected first to initiate the fracture. A less viscous acid fluid such as HCl is injected afterwards into the more viscous pad fluid. Since the displacing acid fluid is less viscous, the well known viscous fingering phenomenon will occur and lead to multiple viscous fingers. The acid in these viscous fingers dissolve more rocks than other regions. There will be more-etched regions and less-etched regions, which are separated by viscous fingers. Li et al. [11] designed a modified Hele-Shaw cell in order to experimentally study viscous fingering during the acid injection period. They used real rock as one fracture wall in the Hele-Shaw cell so that the reaction between acid and rock can be considered. One of their experiment results is shown in **Fig. 4b** where the dark part is the dyed acid fluid.

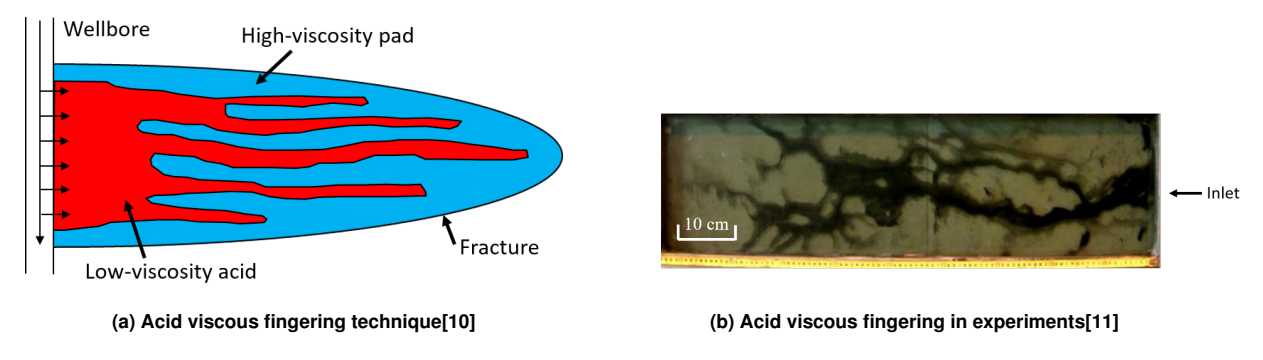


Figure 4: Acid viscous fingering in acid fracturing

Designing acid fracturing jobs requires modeling of the following two processes: (1) injecting pad fluid to initiate the fracture, and (2) injecting acid to create rough fracture surfaces and form acid fracture conductivity. The first process can be modeled using a hydraulic fracture propagation simulator. The second process needs a model to account for the acid flow and reactive transport inside the fracture. Ben-Naceur and Economides[12] coupled a 2D/pseudo 3D fracture model with an acid transport simulator. The model allowed the simulation of both multi-stage injection treatments and gelled acid treatments. They approximated the unstable flow due to viscous fingering by a one-dimension fractional flow similar to the K-factor theory[13]. Gdanski and Lee[14] also developed an acid fracturing simulator which incorporated fracture geometry, temperature calculations and acid spending. Lo and Dean coupled 2D fracture models and acid transport with the assumption of an infinite reaction rate. Settari[15] developed a comprehensive acid fracturing model that solved for 2D/pseudo 3D fracture geometry, leakoff, heat transfer and acid transport. This model accounted for multiple fluids, mass transfer controlled acidizing, reaction kinetics controlled acidizing, and leakoff due to wormholing in the matrix. Settari et al.[16] developed a 2D acid transport model which accounted for acid concentration along the fracture width direction. Romero et al.[17] developed a 3D acid transport model coupled with a pseudo 3D hydraulic fracturing simulator. Previous work did not directly calculate the change of fracture geometry, especially the fracture width due to acid etching. Mou et al.[8] developed an intermediate-scale acid transport model which accounted for fracture face dissolution by acid. In this model, the fracture conductivity was calculated directly from rough acid-etched fracture surfaces. Li et al.[11] modeled acid fingering during acid fracturing. They did not consider the reaction between acid and carbonate rock in their model. Mineral dissolution is also well studied in the geoscience community. Starchenko et al. [18] developed a fracture dissolution simulator based on the OpenFOAM library[19]. They modeled flow, reactive transport inside the fracture and the change of fracture geometry. Starchenko and Ladd[20] studied different fracture dissolution regimes by running numerical simulations under different scenarios of flow and reactive transport.

In this paper, we present a modeling study on acid transport with the viscous fingering effect in acid fracturing treatments. Our mathematical model considers the following processes: (1) the fluid flow inside

the fracture, (2) acid transport and polymer transport, (3) mineral dissolution at the fracture surface and (4) the change of fracture morphology. A numerical simulator has been developed based on the OpenFOAM library [19] to solve the mathematical model. The effect of viscous fingering on acid fracture conductivity will be studied through numerical simulations.

#### **Mathematical Model**

This study focuses on the acid injection period after the pad fluid has been pumped to initiate and propagate the fracture. The fracture is assumed not to propagate when injecting the acid into the fracture. The fracture domain is illustrated in **Fig. 5** where the fracture width is exaggerated for the purpose of illustration. Six boundary faces are defined: (1) inlet, (2) outlet, (3) top face, (4) bottom face, and (5) two fracture wall faces. The mineral of the reservoir formation is calcite. The pad fluid is a polymer solution while the acid fluid is a hydrochloric acid (HCl) solution.

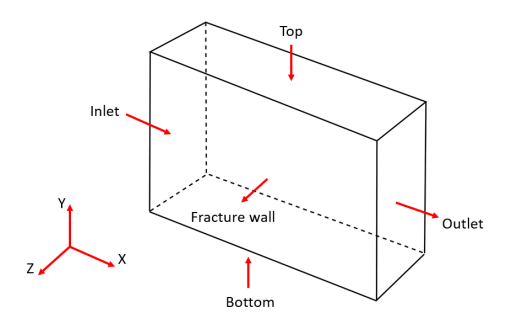


Figure 5: Illustration of fracture domain

## **Model Assumptions**

- 1. There is only aqueous phase in the open fracture. The aqueous phase fluid is incompressible Newtonian fluid.
- 2. The fluid density is constant and independent of concentrations of acid and polymer.
- 3. Gravity is not considered.
- 4. The fluid flow in the fracture is laminar flow.
- 5. Acid leak-off from the fracture to the surrounding reservoir is ignored.

#### Fluid Flow Model

The momentum equation is the incompressible Navier-Stokes equation as shown in **Eq. (1)**. Since the acid etching is slower than the fluid motion, the momentum equation is assumed to be steady-state for each time step. During the acid injection period, the velocity field still changes due to changes in fluid composition.

$$\rho(\mathbf{u} \cdot \nabla \mathbf{u}) = -\nabla p + \mu \nabla^2 \mathbf{u} \tag{1}$$

where  $\rho$  is the fluid density, **u** is the fluid velocity, *p* is the fluid pressure and  $\mu$  is the fluid viscosity. The continuity equation of the aqueous phase fluid is

$$\nabla \cdot \mathbf{u} = 0 \tag{2}$$

The velocity field  $\mathbf{u}$  can be resolved by solving the coupled momentum equation  $\mathbf{Eq.}$  (1) and continuity equation  $\mathbf{Eq.}$  (2).

The fluid flow model is closed by the following boundary conditions

$$\mathbf{u} = \mathbf{u}_{\text{inj}} \qquad \text{inlet} \qquad (3)$$

$$p = p_{\text{out}}$$
 outlet (4)

$$\mathbf{u} = 0$$
 top/bottom/fracture faces (5)

A specific flow rate  $\mathbf{u}_{\text{inj}}$  is maintained at the inlet boundary while a specific pressure  $p_{\text{out}}$  is defined at the outlet boundary. No slip boundary conditions are applied at the other boundaries.

# **Acid Transport Model**

In this paper, we consider HCl solution as the acid fluid. Since it is the proton  $(H^+)$  that dissolves the rock, we only track the  $H^+$  concentration in the aqueous phase fluid, which is described by the advection-diffusion equation

$$\frac{\partial c_1}{\partial t} + \nabla \cdot (\mathbf{u}c_1) - \nabla \cdot (\mathbf{D}_1 \nabla c_1) = 0 \tag{6}$$

where  $c_1$  is the molar concentration of H<sup>+</sup> and  $\mathbf{D}_1$  is the H<sup>+</sup> diffusion-dispersion coefficient.

The boundary conditions of the acid transport model are defined as below.

$$(\mathbf{u}c_1 - \mathbf{D}_1 \nabla c_1) \cdot \mathbf{n} = (\mathbf{u}_{\text{inj}} \cdot \mathbf{n})c_1^{\text{inj}} \qquad \text{inlet}$$

$$-\mathbf{D}_1 \nabla c_1 \cdot \mathbf{n} = 0 \qquad \text{outlet/top/bottom faces} \tag{8}$$

$$-\mathbf{D}_1 \nabla c_1 \cdot \mathbf{n} = R(c_1)$$
 fracture faces (9)

where **n** is the outward normal vector at boundaries,  $c_1^{\text{inj}}$  is the injected acid concentration (i.e. H<sup>+</sup> molar concentration) at the inlet and  $R(c_1)$  is the reaction rate at the fracture faces.

At the inlet, the acid fluid with a specific acid concentration  $c_1^{\rm inj}$  is injected. The zero gradient boundary condition is defined at the outlet, top and bottom faces. At the fracture faces, the amount of H<sup>+</sup> transported to the fracture face is consumed by dissolving the calcite mineral.

The reaction rate between calcite (CaCO<sub>3</sub>) and HCl is described by a linear rate law

$$R(c_1) = kc_1 \tag{10}$$

where *k* is the reaction rate constant.

The initial condition needs to be given to complete the acid transport model.

$$c_1(t=0) = c_1^0 (11)$$

where  $c_1^0$  is the initial molar concentration of  $\mathbf{H}^+$ .

#### **Polymer Transport Model**

The concentration of the polymer in the aqueous solution is commonly described as the mass fraction. The unit of mass fraction is weight percentage and denoted by wt%. The polymer transport is modeled by the advection-diffusion equation

$$\frac{\partial c_2}{\partial t} + \nabla \cdot (\mathbf{u}c_2) - \nabla \cdot (\mathbf{D}_2 \nabla c_2) = 0 \tag{12}$$

where  $c_2$  is the mass fraction of the polymer and  $D_2$  is the polymer diffusion-dispersion coefficient.

The boundary conditions of the polymer transport model are described as below.

$$(\mathbf{u}c_2 - \mathbf{D}_2 \nabla c_2) \cdot \mathbf{n} = (\mathbf{u}_{\text{inj}} \cdot \mathbf{n}) c_2^{\text{inj}} \qquad \text{inlet}$$

$$-\mathbf{D}_{2}\nabla c_{2}\cdot\mathbf{n}=0$$
 outlet/top/bottom/fracture faces (14)

where  $c_2^{\text{inj}}$  is the injected polymer mass fraction at the inlet.

In this paper,  $c_2^{\text{inj}} = 0$  since no polymer is injected at the inlet. The zero gradient boundary condition for  $c_2$  is defined at other faces.

The initial condition needs to be given to complete the polymer transport model.

$$c_2(t=0) = c_2^0 (15)$$

where  $c_2^0$  is the initial mass fraction of polymer.

# **Acid Etching Model**

Since the acid dissolves the calcite mineral at the fracture surface, the domain of the fracture will be enlarged accordingly. The mesh motion is governed by the solid conservation equation.

$$c_s \frac{d\mathbf{r}}{dt} = \alpha R(c_1)\mathbf{n} \tag{16}$$

where  $c_s$  is the molar density of the calcite mineral,  $\mathbf{r}$  is the point vector on the fracture surfaces, and  $\alpha$  is the stoichiometric conversion coefficient, defined as moles of calcite dissolved per mole of acid reacted. The  $\alpha$  is 0.5 for the reaction between HCl and CaCO<sub>3</sub>.

#### **Polymer Viscosity Model**

Here we assume that the viscosity of the polymer solution is a function of polymer concentration  $c_2$ . The effects of non-Newtonian behavior and salinity are not considered here. Our polymer viscosity model is modified from the Flory-Hugging equation[21].

$$\mu = \mu_w \left[ 1 + A_1 c_2 + A_2 c_2^2 + A_3 c_2^3 \right] \tag{17}$$

where  $\mu_w$  is the water viscosity,  $A_1$ ,  $A_2$  and  $A_3$  are model parameters obtained from fitting the experimental data.

#### Algorithm for Solving the Coupled System

The solution algorithm is presented in **Fig. 6**. For each time step, the Navier-Stokes flow is solved first. The acid transport and polymer transport are then solved based on the new velocity field. The new acid concentration field is used to compute the amount of mineral dissolution. The fracture geometry is updated accordingly. The fluid viscosity is updated using the new polymer concentration field. This process is repeated until the final time.

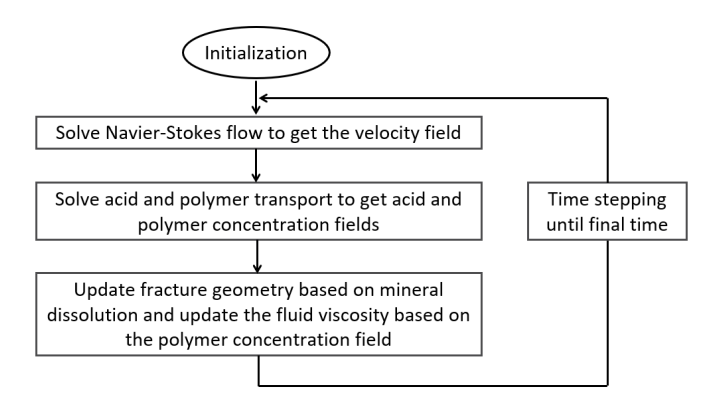


Figure 6: Solution algorithm flowchart

# **Results**

In this section, we conducted numerical simulations based on the developed 3D acid transport model to study the acid etching process in the fracture. We first investigated the viscous fingering phenomenon occurring in the acid fracturing treatment. Then we analyzed the effects of pad fluid viscosity and acid injection rate on acid fracture conductivity when the pad fluid is a polymer fluid.

#### **Effect of Viscous Fingering**

The fracture size in this study is at the lab scale. The initial fracture domain is shown in **Fig. 7**. The acid is injected through a perforation zone at the inlet boundary. The length and the width of the perforation zone are 0.6 cm and 0.1 cm respectively. Periodic boundary conditions are applied at the top and bottom boundary faces. Two cases are set up in order to study the effect of viscous fingering on acid etching in the fracture. The only difference between two cases is the type of pad fluid. The pad fluid of the first case is water (i.e.  $c_2^0 = 0$ ) while the pad fluid is a 0.2422 wt% polymer solution (i.e.  $c_2^0 = 0.2422$ ) in the second case. The initial viscosity of polymer solution, denoted by  $\mu^0$ , in the second case is 50 cP. **Fig. 8** shows how the polymer fluid viscosity changes with the polymer concentration, which is characterized by **Eq. 17**. The injected acid is a 10 wt% HCl solution. The input data for the numerical simulations is shown in **Table 1**. The final time for both cases is 219 min. Since the inertia effect is not obvious in this setup, the inertia term is dropped from **Eq. 1** even though our simulator can solve the full Navier-Stokes equation as shown in (**Eq. 1**).



Figure 7: Initial fracture domain

Parameter	Symbol	Units	Value
Fracture length	L	cm	50
Fracture height	Н	cm	25
Fracture width	W	cm	0.1
Kinetic reaction rate constant	k	cm/s	0.15
Acid diffusion coefficient	$D_1$	cm <sup>2</sup> /s	2.5e-5
Injection velocity	$u_{\rm inj}$	cm/s	0.1
Water viscosity	$\mu_w$	cР	1
Polymer viscosity model parameter	$A_1$	-	35
Polymer viscosity model parameter	$A_2$	-	435
Polymer viscosity model parameter	$A_3$	-	1055
Water density	$\rho_w$	g/cm <sup>3</sup>	1
Injected acid concentration	$c_1^{\rm inj}$	mol/L	2.74
Calcite rock molar concentration	$c_s$	mol/L	27

Table 1: Input data for numerical simulations

#### Case without polymer

In this case, the pad fluid is water. The fluid viscosity does not change along the acid injection. The fields of acid concentration, fracture width and fluid velocity at the final time are shown in Fig. 9 where

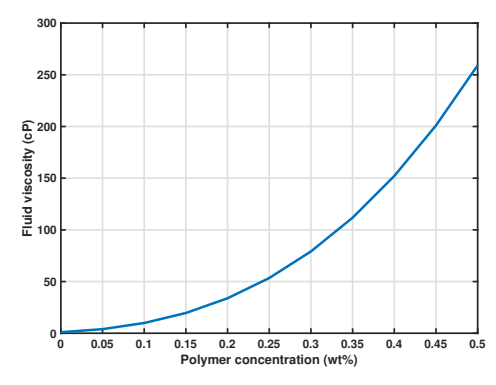


Figure 8: Polymer fluid viscosity as a function of polymer concentration

the inlet is located at the bottom. The acid concentration field is always plotted on the middle slice of the fracture in this paper by default. The unit of acid concentration is converted to weight percentage. In this paper, the plots of velocity fields always show the velocity component along the fracture length direction which is denoted by Ux since Ux mainly determines the acid penetration in the fracture. **Fig. 9a** shows that most of the acid is spent near the fracture inlet. The increase in the fracture width is limited near the inlet. The etched fracture length is relatively short. Most of the fracture is left un-etched and will be closed after the acid injection. The overall acid fracture conductivity in this case is expected to be low.

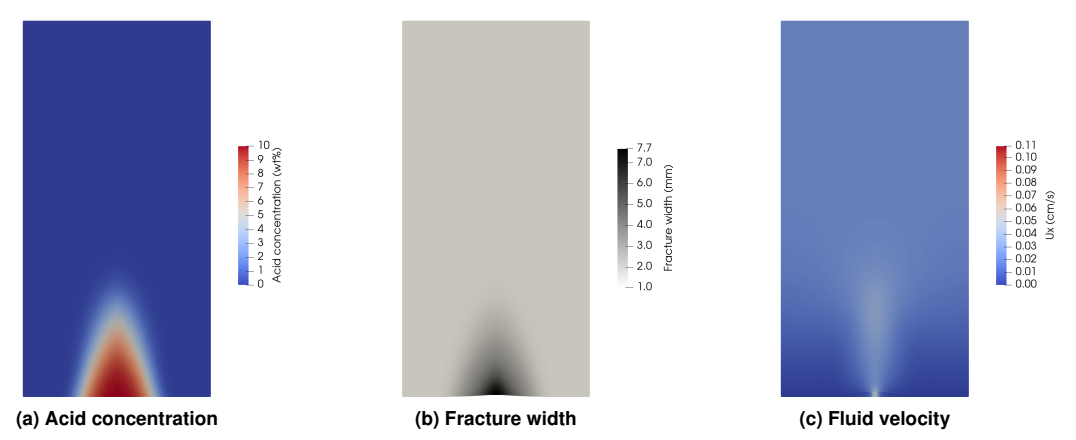


Figure 9: Fields of acid concentration, fracture width and fluid velocity in the case without polymer

#### Case with polymer

In this case, the pad fluid is a polymer solution. The fluid viscosity changes when injecting the acid. The fields of acid concentration, fracture width and fluid velocity at the final time are shown in **Fig. 10**. A contour line of 0.1 wt% acid concentration is plotted to track the acid concentration front while a contour line of 1.01 mm fracture width is plotted to track the acid etching front. Acid concentration fronts and acid etching fronts at the final time are compared between two cases: (1) the case without polymer and (2) the case with polymer. The comparisons are shown in **Fig. 11**. By default, acid concentration fronts and acid etching fronts are represented by the same contour lines in following sections.

In the case with polymer pad fluid, a high-conductivity channel develops in the middle of the fracture due to differential acid etching. Compared to the case without polymer, the etched fracture length is longer and the overall acid fracture conductivity is higher in this case.

The difference in the acid etching patterns from the two cases is caused by the effect of the viscous fingering phenomenon. The velocity field in the fracture is largely dependent on the fluid viscosity field. The velocity component along the fracture length direction from the two cases is shown in **Fig. 9c** and

Fig. 10c respectively. The velocity field in Fig. 9c is more uniform than that in Fig. 10c because the viscosity field is uniform in the case without polymer.

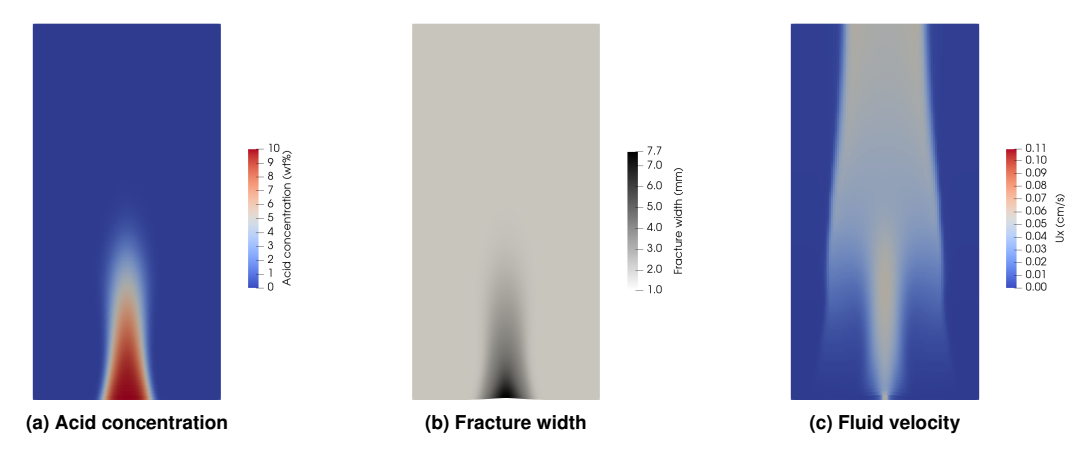


Figure 10: Fields of acid concentration, fracture width and fluid velocity in the case with polymer

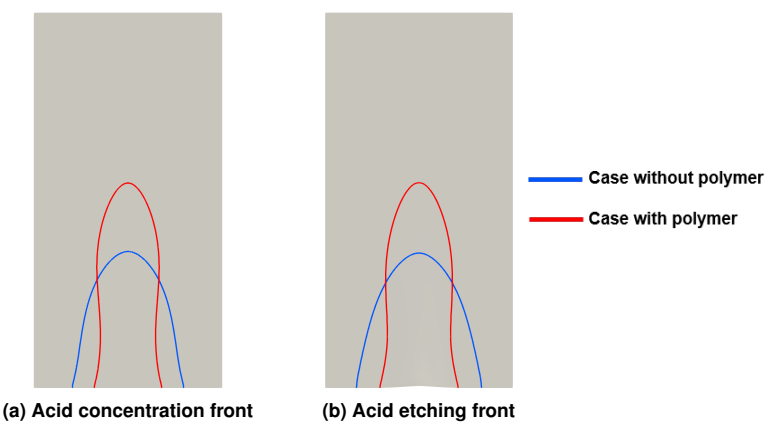


Figure 11: Comparisons of acid concentration fronts and acid etching fronts between (1) the case without polymer and (2) the case with polymer

The effect of the viscous fingering phenomenon on the acid etching process can be examined by tracking the evolution of the fluid viscosity and fluid velocity in the fracture. The fluid viscosity and fluid velocity at different time levels are shown in **Fig. 12**. Early in the process of acid injection (e.g., t = 22 min), the acid is injected through the perforation zone in the middle of the inlet. Since the acid viscosity is smaller than the polymer viscosity, the fluid viscosity in the mixing zone is smaller than the surrounding polymer fluid. The initial viscous fingering is triggered by the localized injection at the perforation. The velocity component along the fracture length direction is larger in the fingering regions. The acid concentration field in **Fig. 12** shows that more acid is diverted into the fingering region because fluid tends to flow into the less viscous area, which makes acid viscous fingering a positive feedback process. Since most acid flows along the center line of the fracture, more calcite is dissolved in the middle of the fracture, leading to the formation of the channel. Because the acid is spent during the dissolution reaction, the acid concentration front is behind the velocity front. The middle channel will be kept open after acid injection even under the closure stress of the formation. When compared to the case without polymer, the acid viscous fingering phenomenon enhances non-uniform acid etching near the fingering region, which is also consistent with previous experimental studies [9, 11].

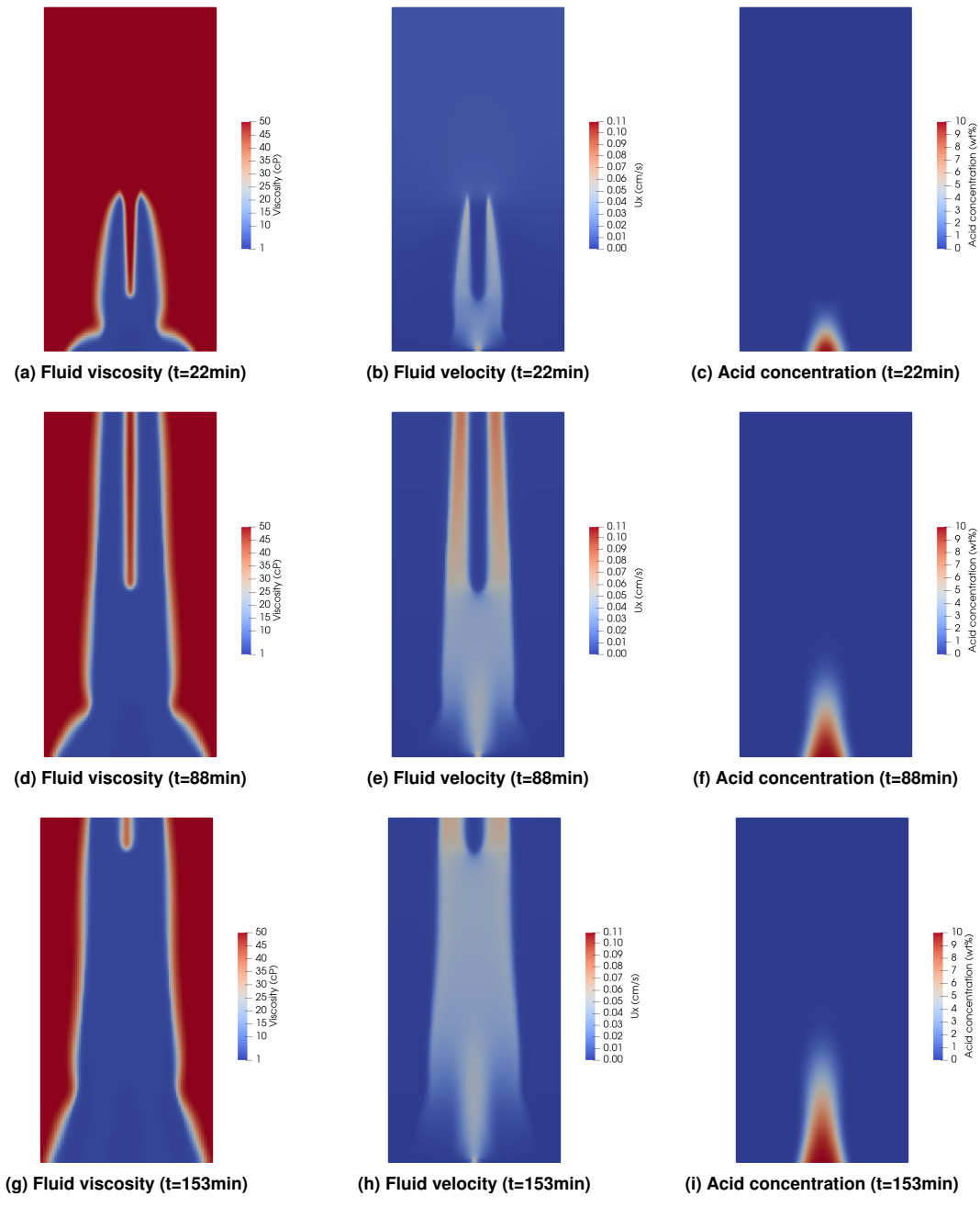


Figure 12: Fields of fluid viscosity, fluid velocity and acid concentration at different time levels in the case with polymer

## **Effect of Pad Fluid Viscosity**

With polymer as the pad fluid, the effect of pad fluid viscosity on the acid etching process is investigated in this section. The same input parameters seen in **Table 1** are used. Three sets of simulations were conducted with three different polymer viscosity values which are 50 cP, 100 cP and 200 cP. The fields of fluid velocity, acid concentration and fracture width at the time level t = 131 min are shown in **Fig. 13**. Acid concentration fronts and acid etching fronts of these three cases at the same time level are compared and shown in **Fig. 14**.

The viscous fingering phenomenon has a larger impact in the case with a more viscous pad fluid. The high velocity area is more constrained in the middle of the fracture and the velocity in the fingering regions also increases as the viscosity increases from 50 cP to 200 cP. Most of the acid is transported along the

fingering area. The high-conductivity channel formed in the middle of the fracture becomes narrower and longer as the viscosity of pad fluid increases. Within the current range of pad fluid viscosities investigated, the larger viscosity ratio of pad fluid viscosity to acid fluid viscosity results in a narrower and longer high-conductivity channel after acid etching. Our current study modeled the fluid viscosity as a function of polymer concentration. The non-Newtonian behavior of the polymer fluid such as shear thinning will be considered in the future work.

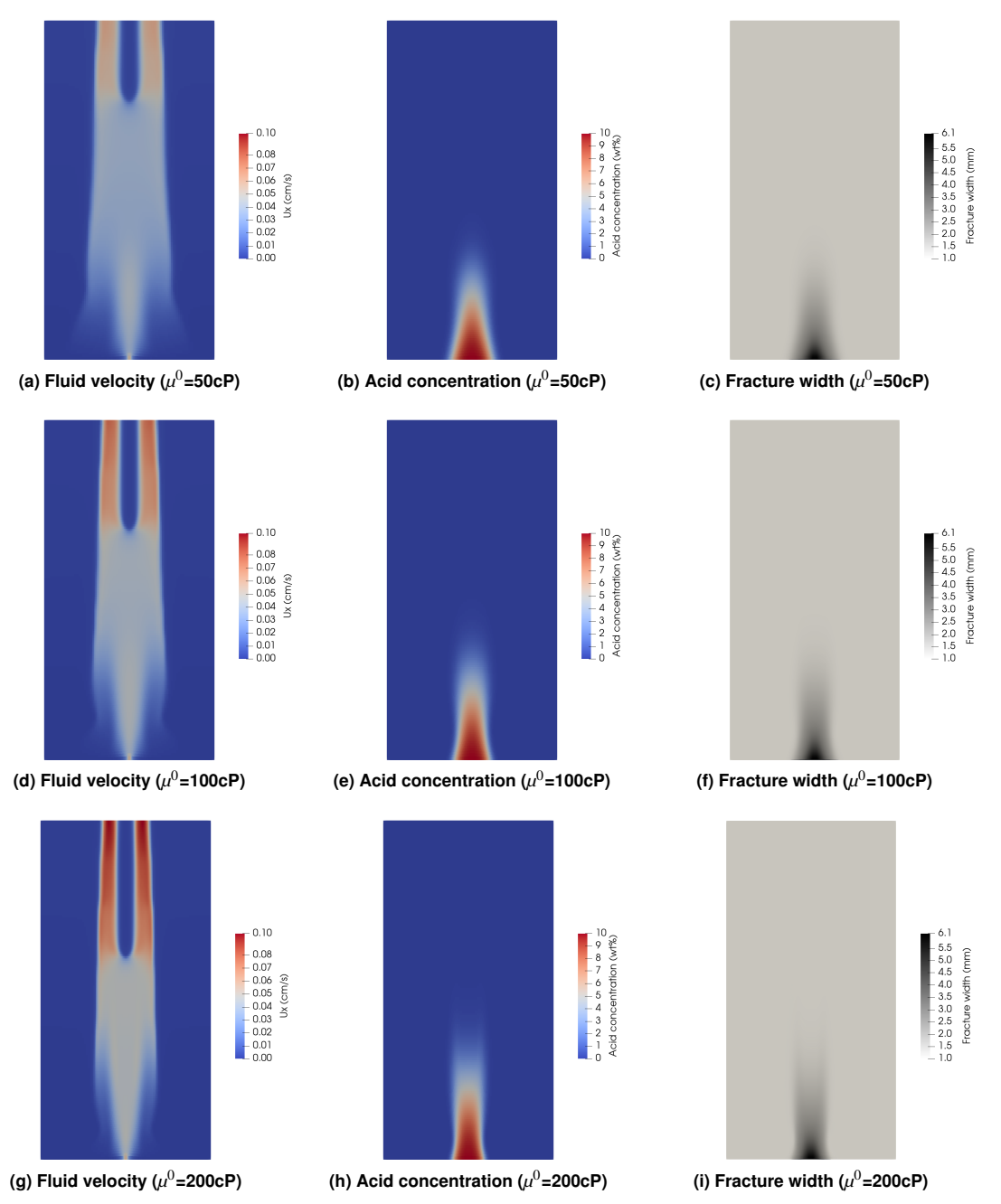


Figure 13: Fields of fluid velocity, acid concentration and fracture width in three cases with different initial pad fluid viscosities

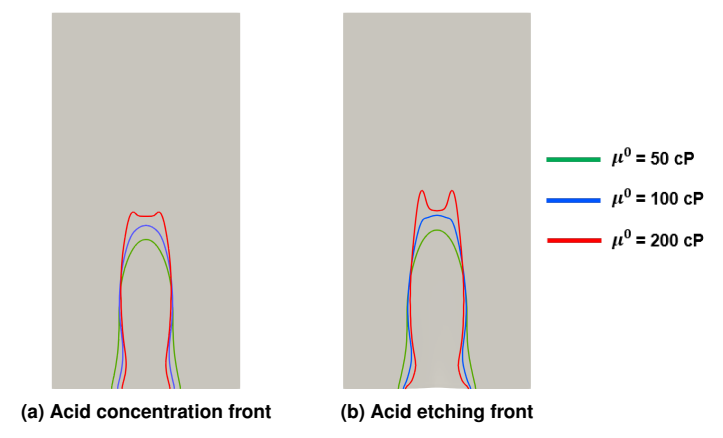


Figure 14: Comparisons of acid concentration fronts and acid etching fronts in three cases with different pad fluid viscosities: (1)  $\mu^0$  = 50 cP, (2)  $\mu^0$  = 100 cP and (3)  $\mu^0$  = 200 cP

#### **Effect of Acid Injection Rate**

In this section, the polymer fluid with the viscosity of 100 cP is the pad fluid. Simulations under different acid injection rates are conducted to study the effect of acid injection rates on the acid etching process. The same input parameters seen in **Table 1** are used except the injection rate parameter. Three different injection rates, denoted by Q, are selected and their values are 0.36 cm<sup>3</sup>/min, 0.72 cm<sup>3</sup>/min and 1.44 cm<sup>3</sup>/min. Since the area of the perforation zone is 0.06 cm<sup>2</sup>, the initial injection velocities for the three cases are 0.1 cm/s, 0.2 cm/s, 0.4 cm/s. During the simulation, the volumetric injection rate is kept constant. As the fracture width and the cross area at the inlet boundary increases due to acid etching, the injection velocity at the inlet will decrease accordingly.

The fields of fluid velocity, acid concentration and fracture width after pumping 63 cm<sup>2</sup> of the acid fluid are shown in **Fig. 15**. Acid concentration fronts and acid etching fronts of these three cases are compared and shown in **Fig. 16**. Based on the field of fluid velocity, the development of viscous fingering is very similar in these three cases with different acid injection rates. As the acid injection rate increases, the fluid velocity in the fingering regions increases. The acid can be transported deeper into the fracture to etch the fracture walls in the case with a higher acid injection rate. Within the current range of acid injection rates investigated, a longer high-conductivity channel can be created in the acid fracturing treatment by increasing the injection rate of the acid fluid.

#### **Discussion**

In this paper, we modeled the non-uniform acid etching process in acid fracturing treatments with viscous fingering. The acid fracturing treatment couples processes of fluid flow, reactive transport and mineral dissolution. This paper is focusing on how the non-uniform fluid velocity field resulting from the viscous fingering phenomenon affects the acid transport and leads to non-uniform acid etching. We investigated the effects of pad fluid viscosity and acid injection rate on acid etching process. In our numerical simulation setup as shown in **Fig. 7**, we have single perforation and periodic boundary conditions on the bottom and top boundary faces. In the future work, multiple perforations will be added in our simulation setup to consider the interference of multiple viscous fingers. Since viscous fingering is an unstable process, one viscous finger may suppress the growth of other neighbor viscous fingers if the pad fluid viscosity or acid injection rate is larger than a threshold. The effects of pad fluid viscosity and acid injection rate on acid etching may not be as monotonic as we observed from current numerical studies.

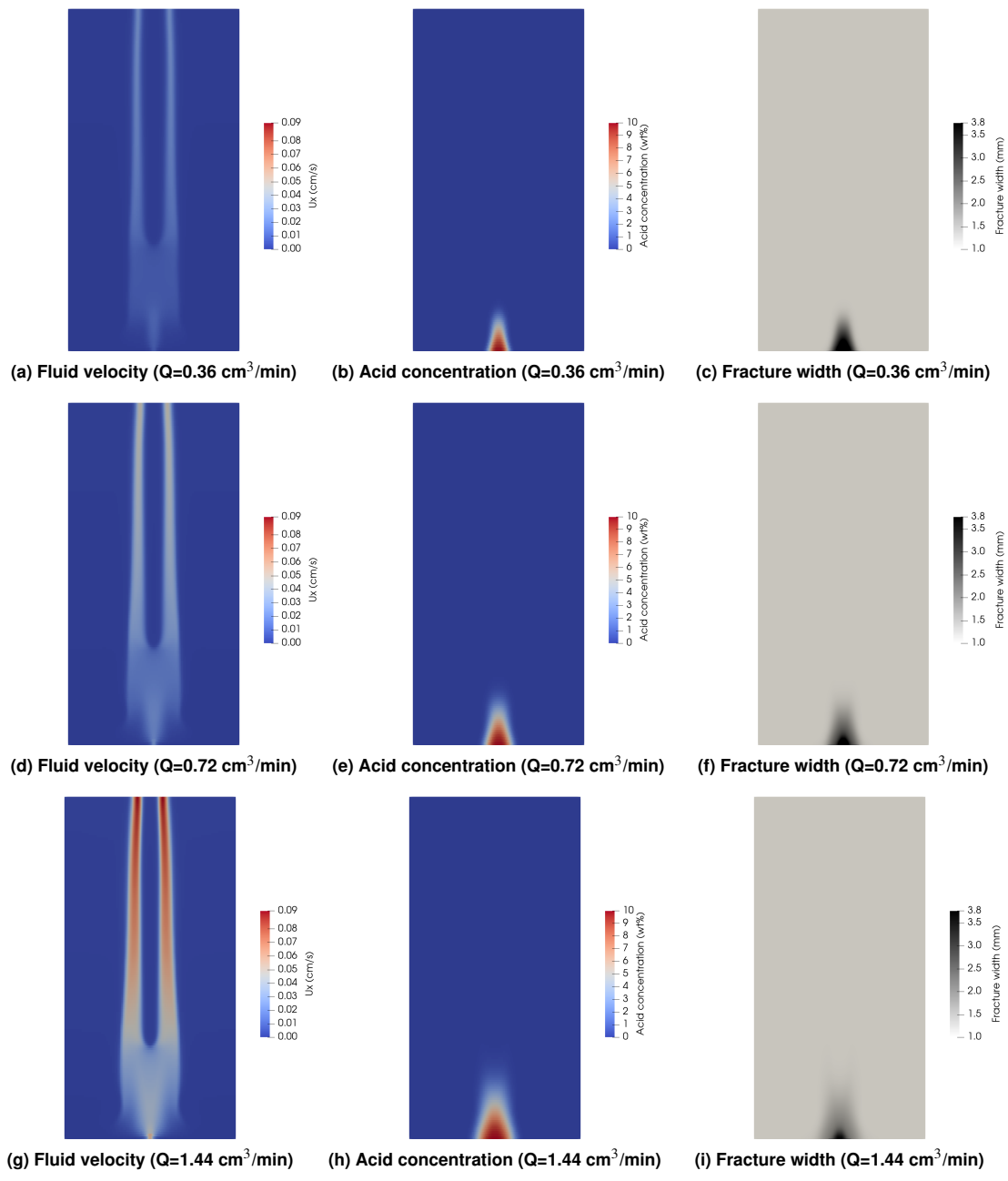


Figure 15: Fields of fluid velocity, acid concentration and fracture width in three cases with different acid injection rates

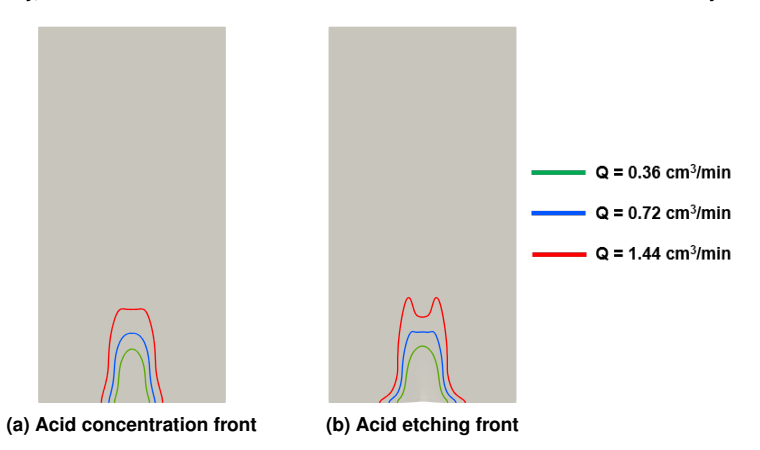


Figure 16: Comparisons of acid concentration fronts and acid etching fronts in three cases with different acid injection rates: (1) Q = 0.36 cm<sup>3</sup>/min, (2) Q = 0.72 cm<sup>3</sup>/min and (3) Q = 1.44 cm<sup>3</sup>/min

# **Conclusions**

This paper presents a mathematical model for acid fracturing treatments with acid viscous fingering. Our model accounts for the fluid flow, acid and polymer transport and fracture dissolution processes. A numerical simulator has been developed to solve the coupled system. The fracture geometry can be obtained at the end of the acid injection period. We compared the acid etching performance in two cases through numerical simulations: (1) where the pad fluid is polymer, and (2) where the pad fluid is water. Our simulation results showed that acid viscous fingering helps achieve non-uniform acid etching, which is also consistent with acid fracturing experiments in the literature. The viscous fingering phenomenon leads to a non-uniform velocity field. The acid is mostly transported to the fingering area. The acid etching activities are constrained in the fingering regions, which results in high-conductivity channels and leaves other parts of the rock not etched. We investigated the effects of the pad fluid viscosity and acid injection rate on acid fracture conductivity when the pad fluid is a polymer fluid. Within current range of polymer viscosities and acid injection rates investigated, the etched fracture length increases with an increasing pad viscosity and acid injection rate. The high-conductivity channel becomes narrower when the ratio of pad viscosity to acid viscosity increases. The developed model can be adopted to assist engineering designs by quantifying effects of various geologic and engineering parameters on acid fracturing treatments.

# **Acknowledgements**

This work was supported by the donors of the American Chemical Society Petroleum Research Fund (Grant #: 59356-ND9).

# **Nomenclature**

 $\rho = fluid density$ 

**u** = fluid velocity

p = fluid pressure

 $\mu$  = fluid viscosity

c = concentration of components

 $\mathbf{D} =$  diffusion-dispersion coefficient of components

 $\mathbf{n} =$  outward normal vector at boundaries

R = reaction rate

k = kinetic reaction rate constant

 $\mathbf{r}$  = point vector on fracture surfaces

 $\alpha =$  stoichiometric conversion coefficient

 $A_1, A_2, A_3 =$  model parameters in polymer viscosity model

# **Subscripts**

1 =acid component

2 = polymer component

w = aqueous phase

s = calcite rock

inj = inlet boundary

out = outlet boundary

# **Superscripts**

0 = initial condition

inj = inlet boundary

#### References

[1] M. Akbar, B. Vissapragada, A. H. Alghamdi, D. Allen, M. Herron, A. Carnegie, D. Dutta, J.-R. Olesen, R. Chourasiya, D. Logan, et al., A snapshot of carbonate reservoir evaluation, Oilfield Review 12 (4) (2000) 20–21.

- [2] M. J. Economides, K. G. Nolte, Reservoir stimulation, Vol. 2, Prentice Hall Englewood Cliffs, NJ, 1989.
- [3] D. McDuff, C. E. Shuchart, S. Jackson, D. Postl, J. S. Brown, Understanding wormholes in carbonates: Unprecedented experimental scale and 3-d visualization, in: SPE Annual Technical Conference and Exhibition, Society of Petroleum Engineers, 2010.
- [4] R. Dong, S. Lee, M. Wheeler, Numerical simulation of matrix acidizing in fractured carbonate reservoirs using adaptive enriched Galerkin method, in: SPE Reservoir Simulation Conference, Society of Petroleum Engineers, 2019.
- [5] R. Dong, M. Wheeler, Simulation of acidizing dissolution front instability in carbonate rocks, in: 2019 AAPG Annual Convention and Exhibition.
- [6] R. Dong, Q. Wang, M. F. Wheeler, Prediction of mechanical stability of acidizing-induced wormholes through coupled hydro-chemo-mechanical simulation, in: 53rd US Rock Mechanics/Geomechanics Symposium, American Rock Mechanics Association, 2019.
- [7] O. Al-Hinai, R. Dong, S. Srinivasan, M. F. Wheeler, A new equi-dimensional fracture model using polyhedral cells for microseismic data sets, Journal of Petroleum Science and Engineering 154 (2017) 49–59.
- [8] J. Mou, D. Zhu, A. D. Hill, Acid-etched channels in heterogeneous carbonates—a newly discovered mechanism for creating acid-fracture conductivity, SPE Journal 15 (02) (2010) 404–416.
- [9] D. Davies, M. Bosma, W. De Vries, Development of field design rules for viscous fingering in acid fracturing treatments: A large-scale model study, in: Middle East Oil Show, Society of Petroleum Engineers, 1987.
- [10] M. Rafie, R. Said, M. Al-Hajri, T. Almubarak, A. Al-Thiyabi, I. Nugraha, E. Soriano, J. Lucado, The first successful multistage acid frac of an oil producer in Saudi Arabia, in: SPE Saudi Arabia Section Technical Symposium and Exhibition, Society of Petroleum Engineers, 2014.
- [11] X. Li, Y. Chen, Z. Yang, F. Chen, Large-scale visual experiment and numerical simulation of acid fingering during carbonate acid fracturing, in: SPE/IATMI Asia Pacific Oil & Gas Conference and Exhibition, Society of Petroleum Engineers, 2017.
- [12] K. Ben-Naceur, M. J. Economides, Design and evaluation of acid fracturing treatments, in: Low Permeability Reservoirs Symposium, Society of Petroleum Engineers, 1989.
- [13] E. Koval, A method for predicting the performance of unstable miscible displacement in heterogeneous media, Society of Petroleum Engineers Journal 3 (02) (1963) 145–154.
- [14] R. Gdanski, W. Lee, On the design of fracture acidizing treatments, in: SPE Production Operations Symposium, Society of Petroleum Engineers, 1989.
- [15] A. Settari, Modeling of acid-fracturing treatments, SPE Production & Facilities 8 (01) (1993) 30–38.
- [16] A. Settari, R. Sullivan, C. Hansen, A new two-dimensional model for acid fracturing design, in: SPE Annual Technical Conference and Exhibition, Society of Petroleum Engineers, 1998.

[17] J. Romero, H. Gu, S. Gulrajani, 3d transport in acid-fracturing treatments: Theoretical development and consequences for hydrocarbon production, SPE Production & Facilities 16 (02) (2001) 122–130.

- [18] V. Starchenko, C. J. Marra, A. J. Ladd, Three-dimensional simulations of fracture dissolution, Journal of Geophysical Research: Solid Earth 121 (9) (2016) 6421–6444.
- [19] Openfoam website, https://www.openfoam.com/.
- [20] V. Starchenko, A. J. Ladd, The development of wormholes in laboratory-scale fractures: Perspectives from three-dimensional simulations, Water Resources Research 54 (10) (2018) 7946–7959.
- [21] P. J. Flory, Principles of polymer chemistry, Cornell University Press, 1953.